Modeling of 3D semiconductor quantum dots in a parallel computing environment

L. R. Ram-Mohan
Departments of Physics, Electrical and Computer Engineering, and Mechanical Engineering,
Worcester Polytechnic Institute,
100 Institute Rd, Worcester, Massachusetts, U.S.A, 01609.
E-mail: LRRAM@wpi.edu

Sathwik Bharadwaj
Departments of Physics,
Worcester Polytechnic Institute,
100 Institute Rd, Worcester, Massachusetts, U.S.A, 01609.
E-mail: sathwik@wpi.edu

Siddhant Pandey
Departments of Physics,
Worcester Polytechnic Institute,
100 Institute Rd, Worcester, Massachusetts, U.S.A, 01609.

C. M. Pierce
Departments of Physics,
Worcester Polytechnic Institute,
100 Institute Rd, Worcester, Massachusetts, U.S.A, 01609.

1 Introduction

Degeneracy in the energy spectrum arises either from geometrical symmetries of the system or from other internal symmetries. A classic example of such degeneracy is given by the hydrogen atom with its Coulomb potential that binds the electron to the proton. The spherical rotational symmetry ($O(3)$) of the Coulomb potential leads to a degeneracy of states of the order $(2\ell + 1)$, where ℓ is the orbital angular momentum quantum number. However, spectroscopic observations showed that for a given principal quantum number n, the different allowed orbital angular momentum states all have the same energy.[1] This additional degeneracy, referred to as "accidental degeneracy", was explained by Pauli[2] by identifying a new conserved vector. Fock[3] further showed that the hydrogen atom has a 4D rotational symmetry, namely of $O(4)$. Thus, symmetries and hidden symmetries play a fundamental role of in the quantum mechanics of physical systems.

As early as in 1990, Shertzer and Ram-Mohan[4] observed that semiconductor quantum wires with a square cross-section exhibit reduction of degeneracy associated with the infinite square well potential. The infinite potential well was shown to have an additional symmetry corresponding to the semi-direct product of C_{4v} and a 1D continuous group of transformations generated by the dynamical operator $(\partial_x^2 - \partial_y^2)$.[5] We can expect that the level degeneracy in the 3D infinite well given by the permutations of (n_x, n_y, n_z) will be richer since the Pythagorean constraint $E \propto n_x^2 + n_y^2 + n_z^2$ can be satisfied in many more ways. The electron's energy $E = (\hbar^2\pi^2/2m^*L^2)(n_x^2 + n_y^2 + n_z^2)$ corresponds to the spherical surface of constant E over the positive octant defined in the number index space, and the degeneracy corresponds to the number of states that fall on such a surface.[6] Within the range of energies that we have explored, we have observed degeneracies of ~ 3000. The reduction in this degeneracy for the cubic finite 3D potential well was already anticipated.[4]

Here, we numerically obtain the energy levels of electrons and holes in cubic quantum dots (QDs) of GaAs embedded in $Ga_{(1-x)}Al_xAs$. This is a prototypical system and our methods apply to any of the II-VI or III-V semiconductor material pairs with Type-I interfaces. We find that the conclusions from 2D carry over to 3D: for cubic QDs, the energy levels for the finite potential are significantly lower than those obtained with the infinite barrier. More striking is the lifting of the degeneracy of certain levels in the energy spectrum of

cubic QDs when a finite-well potential is used.
In Sec. 2, we use finite element analysis (FEA) to solve Schrödinger's equation in the effective-mass approximation within a parallel computing environment. Here, the emphasis is on getting high accuracy for the eigenvalues and eigenfunctions. We show that the use of Hermite interpolation polynomials delivers this; the interface boundary conditions with the additional derivative degrees of freedom (DoF) in the Hermite interpolation can lead to serious book-keeping issues while implementing jump conditions for the derivatives of wavefunctions. This is readily overcome using a novel and unique way of using Fermi-function smoothing described later in this section. In Sec. 3, we use group representation theory to predict which of the accidental degeneracies present in the infinite cubic well are lifted when a finite barrier is used. In Sec. 4, we discuss results obtained through FEA and investigate splitting of energy levels in the presence of an external electric and magnetic field. The concluding remarks are presented in Sec. 5. As a final note, FEA transcends geometrical constraints rather cleanly, and QDs of any shape may be considered for future applications.

2 Finite element analysis of cubic QDs

In the envelope-function approximation (EFA), the charge carrier's envelope function $\psi(x,y,z)$ satisfies Schrödinger's equation with a non-separable potential $V(x,y,z)$ corresponding to a finite barrier height [7],

$$\left[-\nabla\left(\frac{\hbar^2}{2m^*}\nabla\right)+V(x,y,z)\right]\psi(x,y,z)=E\,\psi(x,y,z), \tag{1}$$

where m^* is the carrier effective mass m_w^* or m_b^* in the quantum dot or the surrounding bulk barrier medium, respectively. The potential is

$$V(x,y,z)=\begin{cases} 0, \text{ for } |x|\le a/2, |y|\le b/2, |z|\le c/2, \\ V_0, \text{ outside.} \end{cases} \tag{2}$$

There is a discontinuity in the potential and the effective mass of the charged carriers at the interface between materials. The continuity of the probability current requires that the wavefunction $\psi(x)$ and the 'mass-derivative' of the wavefunction $(1/m^*)\psi'(x)$ be continuous.[8] The input parameters for the effective masses and band offsets of conduction electrons, heavy holes, and light holes in GaAs and in $Ga_{(1-x)}Al_xAs$ are well known.[9] The FEA employing the action integral formulation[10] is used to evaluate the energies and eigenfunctions. FEA is a generalized variational approach in which we divide the physical domain of interest into several small elements. Within each element, we express the envelope function as a linear combination of interpolation polynomials multiplied by as-yet undetermined coefficients that correspond to the value of the wavefunction at the vertices (nodes) of the elements that are usually tetrahedra or cubes in 3D. We use Hermite interpolation polynomials, as opposed to Lagrange polynomials, for which the expansion coefficients are function values and also its derivatives at the nodes.[10] We see a substantial increase in the accuracy of eigenvalues since we have the additional derivative continuities across the elements. The global envelope function is constructed by summing contributions from all elements and ensuring the function value and its derivatives are continuous across the element.[10] Since the finite element approach may be viewed as the discretization of the action integral we define the action from which Eq. (1) is derivable to be

$$\mathcal{A}/T=\int_V d^3r\,\left[\nabla\psi^*\cdot\,\frac{\hbar^2}{2m^*}\,\nabla\psi+\psi^*\,\left(V(x,y,z)-E\right)\,\psi\right]. \tag{3}$$

We are solving here the time-independent problem so that the time integral over the range $[0,T]$ in the action is simply T. Dirichlet boundary conditions are implemented at the periphery of the physical region. In Fig. 1, we show the convergence of the error in the eigenvalues of the ground and first excited state for different interpolation polynomials. Clearly, the Hermite interpolations yield more accurate results than the typical Lagrange interpolation polynomials. In the case of finite barriers, there is a discontinuity in the potential and effective mass of the charge carriers at the interface between materials. Traditionally, while using Hermite finite elements the continuity of the effective mass derivatives is ensured by patching the corresponding row vectors.[4] But this is a computationally expensive and slow process especially in a

parallel computing environment in 3D. We tackle this problem by representing the step function by a Fermi function. Thus the effective mass is given by

$$m^*(x,y,z) = m_b^* - (m_b^* - m_w^*)\left[\left(1+\exp\left[\frac{\left(x+\frac{a}{2}\right)\left(x-\frac{a}{2}\right)}{\delta^2}\right]\right)^{-1}\times \left(1+\exp\left[\frac{\left(y+\frac{b}{2}\right)\left(y-\frac{b}{2}\right)}{\delta^2}\right]\right)^{-1}\left(1+\exp\left[\frac{\left(z+\frac{c}{2}\right)\left(z-\frac{c}{2}\right)}{\delta^2}\right]\right)^{-1}\right]. \quad (4)$$

Similarly, the confining potential is defined by

$$V(x,y,z) = V_0\left[1-\left(1+\exp\left[\frac{\left(x+\frac{a}{2}\right)\left(x-\frac{a}{2}\right)}{\delta^2}\right]\right)^{-1}\left(1+\exp\left[\frac{\left(y+\frac{b}{2}\right)\left(y-\frac{b}{2}\right)}{\delta^2}\right]\right)^{-1}\times \left(1+\exp\left[\frac{\left(z+\frac{c}{2}\right)\left(z-\frac{c}{2}\right)}{\delta^2}\right]\right)^{-1}\right]. \quad (5)$$

Here δ is the smoothing parameter, or the "temperature" in the Fermi function, which controls the smoothing of the interfaces. By systemically decreasing the parameter δ, we mimic the finite barrier potential with a discontinuity. The most important benefit of this smoothing is that the properties of the function are the same on either side of the interface at any energy so that there are no jump-conditions to implement in the calculations. We have verified this and the accuracy obtained in several test calculations.

Variation of the discretized action in Eq. (3) leads to a generalized eigenvalue matrix equation of the form $A\,v = EB\,v$, where, A and B are sparse matrices of dimension equal to the total DoF and v is the eigenvector corresponding to the eigenvalue E. We solve this equation within a parallel computing environment.[11, 12, 13] We use the Krylov-Schur algorithm as implemented in SLEPc.[14] Here, we employ a spectral transformation by a shift-invert operator. The solver works with an equation of the form $(A-\lambda B)^{-1}\,B\,v = \theta\,v$, where, λ is the shift parameter. Energy eigenvalues are computed internally from the relation $E = \lambda + 1/\theta$. This procedure augments the convergence of eigenvalues near λ since the eigenvalues θ of the shift-invert operator are largest in magnitude for those energies in the vicinity of λ.[12] In the case of linear Lagrange interpolation polynomials, with 50 processors, matrices of dimensions 27000×27000 are assembled in 0.6 minutes and diagonalized in 2.9 minutes. On the other hand, using the quintic Hermite interpolation polynomials, with the same number of processors, matrices of the same dimensions are assembled in 70.0 minutes and diagonalized in 10.2 minutes. We pay the price for having to go through more number of loops while using the Hermite interpolation polynomials. This increase in time can be reduced by optimizing the number of processors used for the calculation.

The matrix bandwidth is defined as the sum of sub- and supra-diagonal arrays together with the main diagonal. For a total of 27000 DoF, the linear Lagrange polynomials utilize a bandwidth of 53987, while the quintic Hermite interpolation polynomials occupy a comparable bandwidth of 53903. The occupancy of a matrix is defined as the percentage of nonzero entries in the matrix. While going from the linear Lagrange to quintic Hermite polynomials there is only a nominal increase in the matrix occupancy from 0.214% to 0.929% for the B matrix and 0.06% to 0.928% for the A matrix. The increase in computational time with the Hermite interpolation calculations is compensated considerably by the higher accuracy delivered as seen in Fig. 1.

3 Degeneracy and point group symmetry

Degeneracies in the energy spectrum arise from geometric symmetries of the system under study. They are equal to the dimensions of the irreducible representations of the corresponding symmetry group.[15, 16] Any other additional degeneracy which cannot be explained by the obvious geometrical symmetry of the system is labeled as accidental degeneracy.

We know that for a three dimensional infinite barrier cubic QD of length L, the energy eigenvalues are given by

$$E(n_1,n_2,n_3) = \left(\frac{\hbar^2\pi^2}{2m^*L^2}\right)\left(n_1^2+n_2^2+n_3^2\right), \quad (6)$$

Figure 1: The convergence of the relative errors in eigenvalues of (a) the ground and (b) the first excited state in the QD for linear Lagrange, quadratic Lagrange, cubic Hermite and quintic Hermite interpolation polynomials are shown for the case of an infinite quantum well of dimensions $200\text{Å} \times 200\text{Å} \times 200\text{Å}$. Using quintic Hermite interpolation polynomials we can reduce the error to 10^{-8} with just 27 elements and 2744 degrees of freedom (DoF), with further reduction in error possible with mesh refinement. The total DoF corresponds to the global matrix dimension

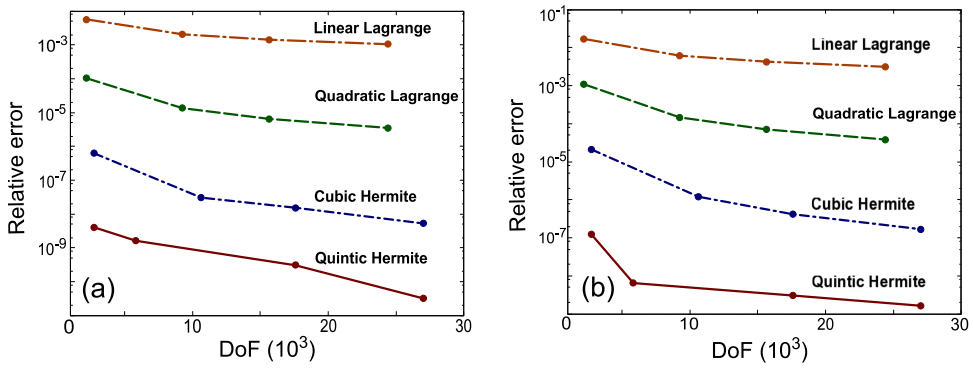

where $n_1, n_2, n_3 \in \mathbb{N}$. Energy eigenvalues reside on the first octant of the number sphere. Note that there are two kinds of degeneracies present. The first kind is due to the permutation of quantum numbers. The second kind are less transparent, occuring when we have the following relation:

$$n_1^2 + n_2^2 + n_3^2 = m_1^2 + m_2^2 + m_3^2, \tag{7}$$

with $n_i \neq m_j$, for $i, j = 1, 2, 3$. Cubic QDs have geometrical octahedral symmetry (O_h). From the character table for the point group O_h, we see that it has only 1, 2 and 3-dimensional representations.[16]

For finite barriers, the potential is non-separable and the accidental degeneracy present in the infinite barrier case is lifted. However, we can still use the infinite barrier quantum numbers for labeling the eigenstates of the finite barrier QD. The states can be written with labels (n_1, n_2, n_3). We require degenerate symmetry adapted wavefunctions to form the basis for their corresponding irreducible representations. We shall thus classify the wavefunctions into their corresponding irreducible representations under O_h. Let G be a group of order g and $\Gamma^{(i)}$ be an l_i-dimensional representation of G. For a group element R in G, its representation is given by an $l_i \times l_i$ square matrix $\Gamma^{(i)}(R)$. Then the projection operator[15] corresponding to $\Gamma^{(i)}$ is given by

$$\mathcal{P}^{(i)} = \frac{l_i}{g} \sum_R \chi^{(i)}(R) \cdot P_R, \tag{8}$$

where $\chi^{(i)}(R)$ is the character and P_R is the operator corresponding to the element R. The projection operator $\mathcal{P}^{(i)}$ projects out a function F on to a part $f^{(i)}$ belonging to the representation $\Gamma^{(i)}$. For a basis function ψ_k then, we can write

$$c_{jk}^{(i)} = \int_V d^3r \; \psi_j^\dagger \left(\mathcal{P}^{(i)} \psi_k \right). \tag{9}$$

If this coefficient is nonzero, the wavefunction ψ_k has a component in the i^{th}-representation and ψ_j is a partner. Once we determine all coefficients, we obtain a new basis function $f^{(i)}$ which is exclusively in the i^{th}-representation. We list out the irreducible representations in O_h corresponding to several quantum numbers in Table 1.

4 Results and discussions

We have used the infinite barrier quantum dot to determine the degeneracy of levels, and the level of accuracy achieved in our numerical calculations with the infinite barrier QD for which the eigenvalues are

Figure 2: We show wavefunctions for states $(1,1,2)$, $(1,2,1)$ and $(2,1,1)$ belonging to the representation T_{1u} of the group O_h. These three states are related by proper rotational operators.

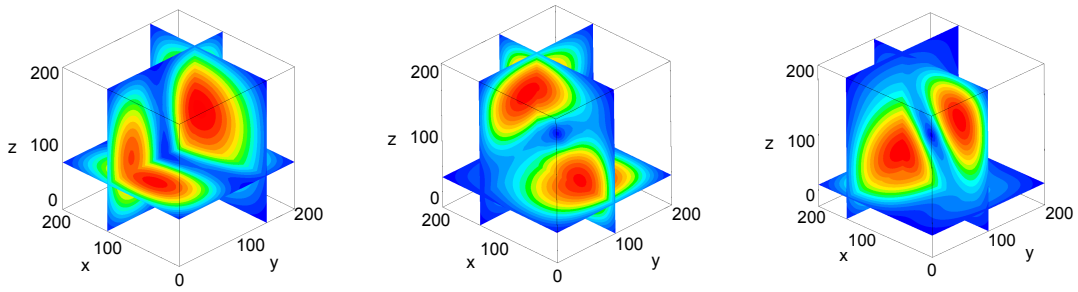

known analytically. We expect that the eigenvalues obtained with a finite well will have almost the same level of accuracy given that the finite well QD calculations are not altering the input numerical values in any significant way. In Table 1, we list the calculated eigenvalues for heavy holes in GaAs/$Ga_{0.3}Al_{0.37}$As cubic QDs of dimensions 200Å $\times$ 200Å $\times$ 200Å.

We represent each eigenstate by a symmetry adapted linear combination of quantum numbers (n_1, n_2, n_3) associated with the infinite well. For comparison we include energy values obtained using the infinite barrier approximation. Note that all of the energy levels are lowered from the values obtained with infinite barriers. Additional accidental degeneracies observed in the case of an infinite barrier are lifted. Clearly, the infinite barrier approximation is invalid in this case. States with symmetric combination of quantum numbers are more bound than others. For example, states corresponding to A_{1g} and A_{2u} have lower energies than that of E_g and E_u respectively. As expected, we have only 1, 2 and 3 level degeneracies. States that were 6 level degenerate in the case of infinite barrier approximation are split into two triplet states for (2 even and 1 odd), or (2 odd and 1 even) combinations of quantum numbers. For all three different odd or even combinations, states will split into 2 singlets and 2 doublets as expected.

In Fig. 2, we have shown wavefunctions for $(1,1,2)$, $(1,2,1)$ and $(2,1,1)$ states projected along three perpendicular planes. These wavefunctions form a basis to the representation T_{1u} of the group O_h.

We can induce level splitting by having an additional perturbation. Thus the symmetry is reduced to one of the subgroup of O_h. The original Hamiltonian H_0 belongs to the irreducible representation A_1 of O_h. The additional perturbation H' may not have the complete O_h symmetry. We determine the new symmetry by finding the subgroup G of maximum dimension in which all the terms of H' form a basis for the irreducible representation A_1 in G. For example, consider an external constant electric field $H' = -eE_0z$ applied to a cubic QD. We note that C_{4v} is the subgroup of maximum dimension in which z is a basis of the representation A_1. Hence O_h symmetry is reduced to C_{4v} symmetry. We decompose all irreducible representations of O_h through direct products of irreducible representations of C_{4v}.[18]

Level splitting is in accordance with group theoretical predictions. For an applied magnetic field $\boldsymbol{B}$ and corresponding vector potential $\boldsymbol{A}$, the perturbing Hamiltonian is given by

$$H' = \frac{e}{m}\boldsymbol{A}.\boldsymbol{p} + \frac{e^2}{2m}|\boldsymbol{A}|^2 - \boldsymbol{\mu}\cdot\boldsymbol{B}, \tag{10}$$

where $\boldsymbol{\mu} = -(e/m)\boldsymbol{S}$ and $\boldsymbol{S}$ is the spin angular momentum. For a constant field $\boldsymbol{B} = B_0\hat{z}$, within the Landau gauge, the vector potential is given by $\boldsymbol{A} = B_0\, x\, \hat{y}$. Hence, H' has terms that transform as xy and x^2. The spin-orbit coupling term contributes only up to a constant value and it has the complete O_h symmetry. By inspection, we see that only the subgroup C_2 has all these terms belonging to its trivial representation A. Here again, all energy levels are split into non-degenerate states as the group C_2 has only one dimensional representations.

Table 1: Heavy-hole energy levels in GaAs/$Ga_{0.63}Al_{0.37}As$ QDs, with $m_w^* = 0.3774m_0$ and $m_b^* = 0.3865m_0$. The typical simplification of using an infinite well to evaluate the energy levels is seen to be in significant error since the finite potential is not separable.

Quantum numbers	Irreducible representation	Energy (meV)	
		$V = 184$	$V = \infty$
$(1,1,1)$	$1A_{1g}$	5.6339074	7.4727812
$(1,1,2)$		11.2717888	14.9455624
$(1,2,1)$	$1T_{1u}$	11.2717888	14.9455624
$(2,1,1)$		11.2717888	14.9455625
$(1,2,2)$		16.9084279	22.4183437
$(2,1,2)$	$1T_{2g}$	16.9084279	22.4183437
$(2,2,1)$		16.9084279	22.4183437
$(1,1,3)+(1,3,1)+(3,1,1)$	$1A_{1g}$	20.6978832	27.4001979
$-(1,1,3)+2(1,3,1)-(3,1,1)$	$1E_g$	20.7001304	27.4001979
$2(1,1,3)-(1,3,1)-(3,1,1)$		20.7001304	27.4001979
$(2,2,2)$	$1A_{2u}$	22.5438146	29.8911249
$(2,3,1)-(2,1,3)$		26.3330823	34.8729792
$(3,2,1)-(1,2,3)$	$1T_{2u}$	26.3330823	34.8729792
$(1,3,2)-(3,1,2)$		26.3330823	34.8729792
$(2,3,1)+(2,1,3)$		26.3345962	34.8729792
$(3,2,1)+(1,2,3)$	$1T_{1u}$	26.3345962	34.8729792
$(1,3,2)+(3,1,2)$		26.3345962	34.8729792
$(1,2,4)-(1,4,2)$		39.6765282	52.3094705
$(2,1,4)-(4,1,2)$	$1T_{2g}$	39.6765282	52.3094705
$(2,4,1)-(4,2,1)$		39.6765282	52.3094705
$(1,2,4)+(1,4,2)$		39.6883222	52.3094705
$(2,1,4)+(4,1,2)$	$1T_{1g}$	39.6883222	52.3094705
$(2,4,1)+(4,2,1)$		39.6883222	52.3094705
$(2,2,4)+(2,4,2)+(4,2,2)$	$1A_{2u}$	45.3002293	59.7822517
$-(2,2,4)+2(2,4,2)-(4,2,2)$	$1E_u$	45.3181042	59.7822517
$2(2,2,4)-(2,4,2)-(4,2,2)$		45.3181042	59.7822517
$(1,3,5)-(1,5,3)+(3,5,1)$ $-(3,1,5)+(5,1,3)-(5,3,1)$	$1A_{1g}$	67.0254522	87.1824696
$(1,3,5)+(1,5,3)+(3,5,1)$ $+(3,1,5)+(5,1,3)+(5,3,1)$	$1A_{2g}$	67.0857917	87.1824696
$2(1,3,5)-(3,5,1)-(5,1,3)$		67.0311478	87.1824696
$2(3,5,1)-(5,1,3)-(1,3,5)$	$2E_g$	67.0311478	87.1824696
$2(3,1,5)-(1,5,3)-(5,3,1)$		67.0805808	87.1824696
$2(1,5,3)-(3,1,5)-(5,3,1)$		67.0805808	87.1824696

5 Conclusions

We have presented calculations based on FEA within a parallel computing environment which provides accurate energy eigenvalues and symmetry adapted wavefunctions for a cubic quantum dot. Such accuracy is necessary to study linear and non-linear optical, electrical and magnetic properties of a quantum dot. We have shown that the infinite barrier approximation leads to serious errors and additional (accidental) degeneracies. We can predict degeneracies in the energy spectrum and symmetries of the wavefunction systematically using Group representation theory. Our method is general and can be easily extended to find the energy spectrum for a quantum dot of any shape and size.

6 Acknowledgments

We thank the Center for Computational NanoScience (CCNS) at WPI for the computational resources used for these calculations. SP and CMP wish to thank WPI for summer research funding.

References

[1] J. J. Sakurai, *Modern Quantum Mechanics* (Addison-Wesley, Reading, MA, 1994).

[2] W. Pauli, Z. Physik **36**, 336 (1926).

[3] V. Fock, Z. Phys. **98**, 145 (1935).

[4] J. Shertzer and L. R. Ram-Mohan, Phys. Rev. B **41**, 14 (1990).

[5] F. Leyvarz, A. Frank, R. Lemus and M. V. Andrez, Am. J. Phys. **65**, 1087 (1997).

[6] F. Reif, *Fundamentals of Statistical and Thermal Physics* (McGraw-Hill, New York, 1965).

[7] G. Bastard, Phys. Rev. B **24**, 5693 (1981); **25**, 7584 (1982); also see L. R. Ram-Mohan, K. H. Yoo, and R. L. Aggarwal, ibid. **38**, 6151 (1988), and references therein.

[8] D. J. BenDaniel and C. B. Duke, Phys. Rev. **152**, 683 (1966).

[9] I. Vurgaftman, J. R. Meyer and L. R. Ram-Mohan, J. Appl. Phys. **89**, 5815–5875 (2001).

[10] L. R. Ram-Mohan, *Finite and Boundary Element Applications in Qunatum Mechanics* (Oxford University Press, New York, 2002).

[11] Satish Balay *et al.*, Argonne National Laboratory, ANL-95/11 - Revision 3.7, 2016. *PETSc Users Manual.*

[12] V. Hernandez, J. E. Roman, and V. Vidal, ACM Trans. Math. Software, **31**, 3, 351–362 (2005).

[13] P. R. Amestoy and I. S. Duff and J.-Y. L'Excellent and J. Koster, SIAM J. on Matrix Analysis and Applications **23**, 1, 15–41 (2006).

[14] V. Hernandez, J. Roman, A. Tomas, and V. Vidal, Universidad Politécnica de Valencia, Tech. Rep. STR-7, 2007. Also see, G. W. Stewart, SIAM J. Matrix Anal. Appl. **23**, 3, 601–614 (2001).

[15] M. Tinkham, *Group Theory and Quantum Mechanics* (Dover Publications, New York, 2003).

[16] M. S. Dresselhaus, G. Dresselhaus and A. Jorio, *Group Theory: Application to the Physics of Condensed Matter* (Springer, Berlin, 2008).

[17] A. O. Hernandez-Castillo and R. Lemus, J. Phys. A: Math. Theor. **46**, 465201 (2013). Also see, F. M. Fernandez, arXiv:1310.5136 [quant-ph].

[18] H. Bethe, Ann. Physik, **3**, 133–206 (1929).